

Cite this article as: Li Xiaohuan, Cui Guowei, Chen Sihan, et al. Effect of Silicon on Precipitates of High-Silicon Austenitic Stainless Steel[J]. Rare Metal Materials and Engineering, 2022, 51(08): 2769-2776.

ARTICLE

# Effect of Silicon on Precipitates of High-Silicon Austenitic Stainless Steel

Li Xiaohuan<sup>1</sup>, Cui Guowei<sup>1</sup>, Chen Sihan<sup>2</sup>, Liang Tian<sup>2,3,4</sup>, Xing Weiwei<sup>2</sup>, Ma Yingche<sup>2</sup>, Wang Ping<sup>1</sup>, Wu Jinming<sup>3</sup>, Li Guobin<sup>4</sup>

<sup>1</sup> Key Laboratory of Electromagnetic Processing of Materials, Ministry of Education, Northeastern University, Shenyang 110819, China; <sup>2</sup> Key Laboratory of Nuclear Materials and Safety Assessment, Institute of Metal Research, Chinese Academy of Sciences, Shenyang 110016, China; <sup>3</sup> State Key Laboratory of Silicon Materials, School of Materials Science and Engineering, Zhejiang University, Hangzhou 310027, China; <sup>4</sup> Zhejiang Xindeda Special Pipe Industry Co., Ltd, Wenzhou 325024, China

**Abstract:** The effect of silicon contents (4wt%~8wt%) on microstructure of high-silicon austenitic stainless steel ZeCor was investigated by XRD, TEM and indentation deformation. Results show that increasing Si content leads to the phase constitute change of ZeCor alloy: the microstructure is single-phase austenite ( $\gamma$  phase) in ZeCor-4wt%Si alloy,  $\gamma$  phase with a small quantity of  $\sigma$ -phase in ZeCor-6wt%Si alloy, and as for the ZeCor-8wt%Si alloy, the main precipitations are  $\text{Cr}_3\text{Ni}_5\text{Si}_2$  phase and a bit  $\sigma$ -phases. In addition, the  $\text{Cr}_3\text{Ni}_5\text{Si}_2$  phase has a higher silicon and nickel content than the  $\sigma$ -phase. The  $\text{Cr}_3\text{Ni}_5\text{Si}_2$  phase with a micro-hardness HV as high as 7840 MPa is a typical hard and brittle phase, and the precipitation of such phase can greatly increase the micro-hardness of the  $\gamma$  matrix in the ZeCor-8wt% Si alloy. The strengthening mechanism of  $\gamma$  matrix in ZeCor alloy is as follows: the solid solution strengthening is the main strengthening mechanism in ZeCor-6wt% Si alloy, while the solid solution strengthening of Si and the precipitation strengthening of  $\text{Cr}_3\text{Ni}_5\text{Si}_2$  greatly increase the micro-hardness of the  $\gamma$  matrix in ZeCor-8wt%Si alloy, and the  $\text{Cr}_3\text{Ni}_5\text{Si}_2$  phases have a great effect.

**Key words:** high-silicon austenitic stainless steel; silicon content;  $\sigma$ -phase; micro-hardness tester;  $\text{Cr}_3\text{Ni}_5\text{Si}_2$  phase

Sulfuric acid is the most widely produced chemical in the world today, with extraordinary range of modern uses in chemical, agricultural, military and medical fields<sup>[1,2]</sup>. Sulfuric acid shows different properties at different concentrations and temperatures<sup>[3]</sup>. At elevated temperatures, high concentration sulfuric acid is highly corrosive, so the sulfuric acid plant corrosion is the main reason for the leakage of equipment in the sulfuric acid manufacturing process. Therefore special attention must be given to the key parts in the production of sulfuric acid<sup>[4]</sup>. In the past, many studies have shown that silicon can improve the corrosion resistance of stainless steel<sup>[5-12]</sup>. For example, in Saramet stainless steel and Sandvik SX stainless steel<sup>[13,14]</sup>, which are widely used in chemical production, the mass fraction of Si reaches 5wt%~6wt%, and its corrosion rate in concentrated sulfuric acid with a concentration greater than 98% at 130 °C is only 0.1 mm/a<sup>[15-23]</sup>. In

the 1970s, the American Lewis Company developed a new nickel-based Lewmet alloy with a Si content reaching 6wt% and the corrosion rate in 120 °C concentrated sulfuric acid is less than 0.1 mm/a. After age-hardening, the hardness (HRC) of the alloy can rise to around 50 and it has been successfully used to manufacture high-temperature concentrated sulfuric acid pumps. American Monsanto company introduced a high-silicon stainless steel ZeCor. Compared with SX, the content of Cr and Ni in this alloy is reduced while the content of Si is increased. The corrosion rate of this steel is less than 0.0254 mm/a in 93%~99% hot sulfuric acid, so it is generally employed in high-temperature concentrated sulfuric acid production. In China, the research and development of high-silicon austenitic stainless steel for high-temperature concentrated sulfuric acid began in the late 1980s. Several high-silicon stainless steels were studied, such as FS-1, C<sub>2</sub>

Received date: August 07, 2021

Foundation item: Postdoctoral Research Funding Project of Zhejiang Province (ZJ2020017)

Corresponding author: Liang Tian, Associate Researcher, Key Laboratory of Nuclear Materials and Safety Assessment, Institute of Metal Research, Chinese Academy of Sciences, Shenyang 110016, P. R. China, E-mail: tliang@imr.ac.cn

Copyright © 2022, Northwest Institute for Nonferrous Metal Research. Published by Science Press. All rights reserved.

(00Cr17Ni15Si4Nb),  $C_4$  (00Cr14Ni14Si4) and XDS, but most of them are cast steel and concentrated in 4wt%~5wt% silicon steel<sup>[24-27]</sup>.

Beside the beneficial effects of Si addition on the corrosion resistance, some problems are also introduced, which will influence part of the mechanical properties of stainless steel<sup>[9,18,28]</sup>. For example,  $\sigma$ -phase,  $\chi$ -phase,  $M_6C$  carbide and  $Cr_3Si$  can be easily found in the steels when silicon contents are high<sup>[29,30]</sup>. Most of these phases are hard and brittle, and have negative effect on the mechanical property of the stainless steels<sup>[31-34]</sup>: the appearance of these precipitations will inevitably lead to the formation of Si-poor and Cr-poor areas in the surrounding area, which is also extremely detrimental to the corrosion resistance of the material. In addition, the Si atoms solubilizes in the matrix, causing the lattice distortion, and the degree of lattice distortion will increase with the increase of the Si content, so the hardness of the matrix will increase, and Si will segregate around the dislocation to form Cottrell atmosphere, which also hinders the movement of the dislocation<sup>[35]</sup>. Therefore, understanding the effect of Si on high-silicon austenitic stainless steel is vital to obtain good corrosion resistance and mechanical properties.

However, little literatures can be found referring to this aspect. In this research, different silicon contents were designed in ZeCor alloy, the microstructure, composition, morphology and micro-hardness of the precipitates and microstructure evolution of ZeCor alloys were studied, and the influence of silicon content on the precipitation mechanism of different types of precipitates was discussed.

## 1 Experiment

ZeCor alloy with varying Si contents (4wt%, 6wt% and 8wt%) were melted in a vacuum induction melting (VIM) furnace, and the mass of the smelted ingot was 25 kg. The diameter of the cast ingot was 120 mm. The measured chemical composition for each alloy is listed in Table 1.

Cylindrical samples with a diameter of 10 mm and a length of 10 mm were sectioned from the center of the ingots by wire electrical discharge, the cross-sections were subsequently ground by manual grinder for polishing, and the surfaces of these samples were corroded for several seconds with the mixed liquor of 30 mL glycerinum+20 mL HF+10 mL HNO<sub>3</sub>. The microstructure of austenitic stainless steels with different Si contents was characterized by optical microscope (OM) and MERLIN Compact scanning electron microscopy (SEM). The precipitates in the ZeCor-Si steels were identified by X-ray diffraction (XRD), which was carried out using Cu K $\alpha$  radiation in a Rigaku D/max 2500PC X-ray diffractometer; 2 $\theta$  angles in the range of 10°~90° were scanned with the step

speed of 1°/min. The sheets with 0.5 mm in thickness were cut and sanded to a thickness of 0.05 mm using sandpapers, then the thin zone was obtained using a double jet electrolytic thinner to get the TEM samples, and the TEM observations were carried out on a JEM-2100F operating at 200 kV. After that, scanning transmission electron microscope (STEM) imaging, energy dispersive spectrometer (EDS) and selected electron diffraction (SAED) were used to further analyze the precipitates in the ZeCor alloy with different Si contents. The micro-hardness was measured by FM-700e micro-hardness tester under a load of 100 g for 15 s.

## 2 Results and Discussion

### 2.1 Microstructure and precipitation phase characterization

Fig. 1 shows the cast microstructure of ZeCor alloy. From Fig. 1a and 1d, it can be observed that only  $\gamma$  phase exists and its grain boundaries are clearly viewed in ZeCor-4wt% Si alloy. However, a large number of black precipitates (marked by I) with fine strips or dots along the grain boundary are observed in ZeCor-6wt% Si alloy (Fig. 1e), and these phases account for 7.65% of the total area (Fig. 1e and Table 2). However, from Fig. 1c and 1f, it can be seen that a lot of gray bulk-like of precipitates (marked by II) appear and these precipitates account for 57.07% of the total area, which greatly reduces the  $\gamma$  matrix and the proportion of the black precipitates decreases a little bit in the ZeCor-8wt% Si alloy (Table 2).

Fig. 2 is SEM microstructures of ZeCor alloy. In ZeCor-4wt% Si alloy, the grain boundaries of  $\gamma$  matrix are clearly identified and no precipitated phase is observed in ZeCor-6wt% Si alloy. The black precipitates I in OM are white in SEM micrograph and formed at the austenite grain boundaries. When the Si content is 8wt%,  $\gamma$  matrix is obviously reduced, and gray bulk-like precipitates II in OM show black in SEM micrograph. The black precipitate II mainly precipitates in the matrix, and the white precipitate I is found between the  $\gamma$  phases and the precipitate II.

These precipitates in the ZeCor alloy were analyzed by XRD. From Fig. 3, it can be observed that precipitate I may be  $\sigma$ -phase, and precipitate II may be  $Cr_3Ni_3Si_2$  phase. The microstructure of ZeCor alloys changes with increasing the Si contents:  $\gamma$  matrix (4wt% Si)  $\rightarrow$   $\sigma$ -phase and  $\gamma$  matrix (6wt% Si)  $\rightarrow$   $Cr_3Ni_3Si_2$  phase,  $\sigma$ -phase and  $\gamma$  matrix (8wt% Si).

In order to further determine the types of precipitation phases in Fig. 2b and 2c, TEM was employed to identify the precipitates in ZeCor-6wt% Si and ZeCor-8wt% Si alloys. According to the SAED patterns in Fig. 4a and 4b, the precipitate

**Table 1** Measured chemical composition of ZeCor alloy with different Si contents (wt%)

Alloy	C	Mn	Si	Cu	Cr	Ni	Mo	P	S	Fe
ZeCor-4wt%Si	0.026	1.95	4.01	1.02	13.8	16.33	1.03	<0.005	<0.003	Bal.
ZeCor-6wt%Si	0.027	1.96	5.93	1.02	13.83	16.19	1.06	<0.005	<0.003	Bal.
ZeCor-8wt%Si	0.028	1.97	8.18	1.01	13.82	16.16	1.05	<0.005	<0.003	Bal.

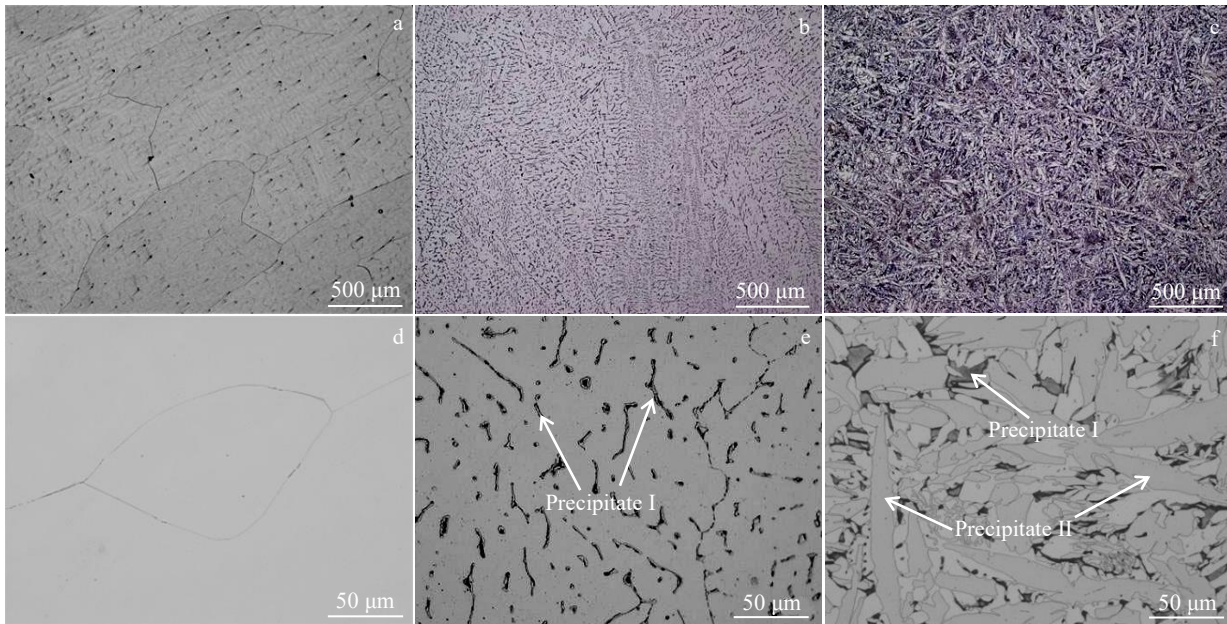


Fig.1 OM microstructures of austenitic stainless steels with different Si contents: (a, d) 4wt%, (b, e) 6wt%, and (c, f) 8wt%

**Table 2 Proportion of different precipitations marked in Fig. 1 in ZeCor alloy (%)**

Alloy	Precipitate I	Precipitate II
ZeCor-6wt%Si	7.65	-
ZeCor-8wt%Si	6.12	57.07

I formed along grain boundary (Fig. 2b) can be identified as the  $\sigma$ -phases, the precipitate II is identified as the  $\text{Cr}_3\text{Ni}_5\text{Si}_2$  phases (Fig. 4f). So, considering that the first emerged phase is  $\sigma$ -phase in ZeCor-6wt%Si alloy, it can be inferred that the increase of Si content will first promote  $\sigma$ -phase precipitation. While in ZeCor-8wt% Si alloy, with higher Si content,  $\text{Cr}_3\text{Ni}_5\text{Si}_2$  phase subsequently precipitates, and meanwhile the amount of  $\sigma$ -phase changes a little with the increase of Si content.

Fig. 5 are microstructures and EDS results of ZeCor alloy with different Si contents. Table 3 is the element contents of the precipitation phases and the matrix counted by EDS. According to Fig. 5 and Table 3, it can be seen that the structure is composed of a single-phase  $\gamma$  matrix without other phases in ZeCor-4wt%Si alloy, in other words, the Si atoms

are solid-dissolved in the  $\gamma$  matrix. The  $\sigma$ -phase (Fig. 5b and 5c) enriched with Si, Cr, Mo alloying elements can be observed in both ZeCor-6wt% Si alloy and ZeCor-8wt% Si alloy, while the Si content in  $\gamma$  matrix is slightly less than 6wt% in ZeCor-6wt%Si alloy (Table 3). As for ZeCor-8wt%Si alloy, the  $\text{Cr}_3\text{Ni}_5\text{Si}_2$  phase is enriched in Si, Cr, Ni elements compared with the  $\sigma$ -phase and  $\gamma$  matrix (Fig. 5c). This is because precipitated  $\text{Cr}_3\text{Ni}_5\text{Si}_2$  phase consumes large amounts of Cr, Mo in the matrix, which results in lower Cr, Mo content in  $\sigma$ -phase. In addition, it can be found from Table 3 that the contents of Si in the matrix of both the ZeCor-6wt% Si alloy and the ZeCor-8wt%Si alloy are about 5wt%, indicating that no matter how high the Si content is, the maximum amount of Si in the matrix is almost unchanged<sup>[36]</sup>. When more than 6wt% of silicon is added to the steel, excess silicon atoms in matrix can be expelled by forming precipitates, such as  $\text{Cr}_3\text{Ni}_5\text{Si}_2$  phase and  $\sigma$ -phases. Studies have also reported that in addition to being solid-dissolved in the  $\gamma$  matrix when silicon is added to stainless steel, part of silicon will exist in the matrix in the form of silicides and silicates<sup>[21,37-41]</sup>.

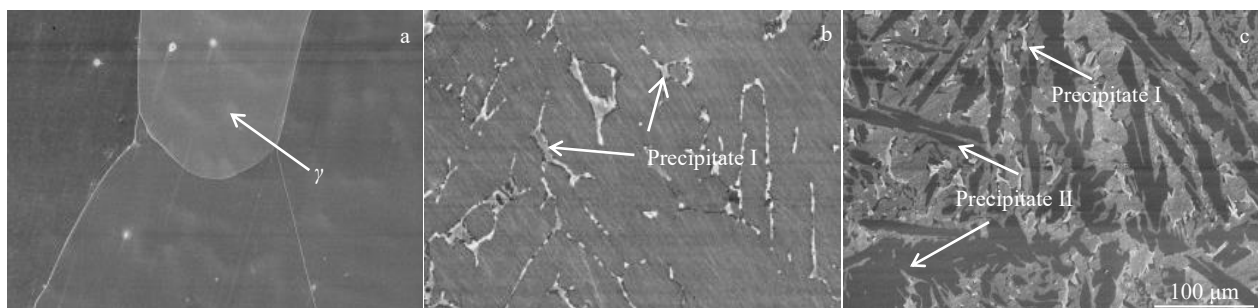


Fig.2 SEM microstructures of ZeCor-4wt%Si (a), ZeCor-6wt%Si (b), and ZeCor-8wt%Si (c)

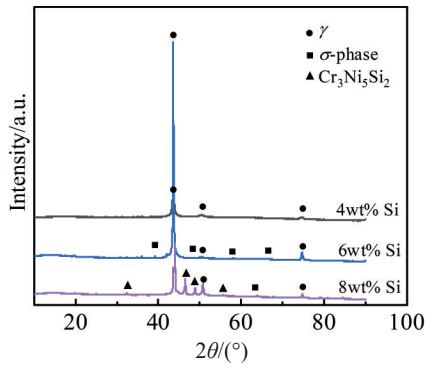


Fig.3 XRD patterns of as-cast ZeCor alloy with different Si contents

## 2.2 Effect of silicon content on the micro-hardness of ZeCor alloy

The micro-hardness test was carried out on the samples, as shown in Fig.6. It can be observed that the micro-hardness of the  $\gamma$  matrix gradually increases when the silicon content is raised from 4wt% to 8wt%. Compared with the micro-hardness of  $\gamma$  matrix in ZeCor-4wt%Si alloy, the micro-hardness of ma-

trix in ZeCor-6wt% Si alloy is approximately improved by 34.3% (~461 MPa). The micro-hardness of  $\gamma$  matrix in ZeCor-8wt% Si alloy is improved by about 51.0% (~911 MPa) compared with the micro-hardness of  $\gamma$  matrix in ZeCor-6wt% Si alloy. As mentioned before, the Si atoms in  $\gamma$  matrix of ZeCor-8wt% Si alloy is not increased significantly (Fig. 6), so the silicon content may not be the main reason for the micro-hardness increment in  $\gamma$  matrix of the ZeCor-8wt% Si alloy.

Fig.7 shows the slip bands around the micro-hardness trace on the matrix and precipitates in three kinds of alloys after indentation deformations. It can be observed that the deformation zone around the indentation is not hindered when squeezed by an external force in ZeCor-4wt% Si alloy, so it has a wide range of slip lines. While in ZeCor-6wt% Si alloy (Fig. 7b), the  $\sigma$ -phases are distributed in  $\gamma$  matrix and act as hard phases<sup>[30,31]</sup>, which hinder the slip movement in the matrix. In ZeCor-8wt% Si alloy, it is obvious that the slip bands in the  $\gamma$  matrix are hindered by the  $\text{Cr}_3\text{Ni}_5\text{Si}_2$  phases, which greatly improves the micro-hardness of the  $\gamma$  matrix (Fig. 7c). Furthermore, the micro-hardness of  $\text{Cr}_3\text{Ni}_5\text{Si}_2$  phase is ~7840

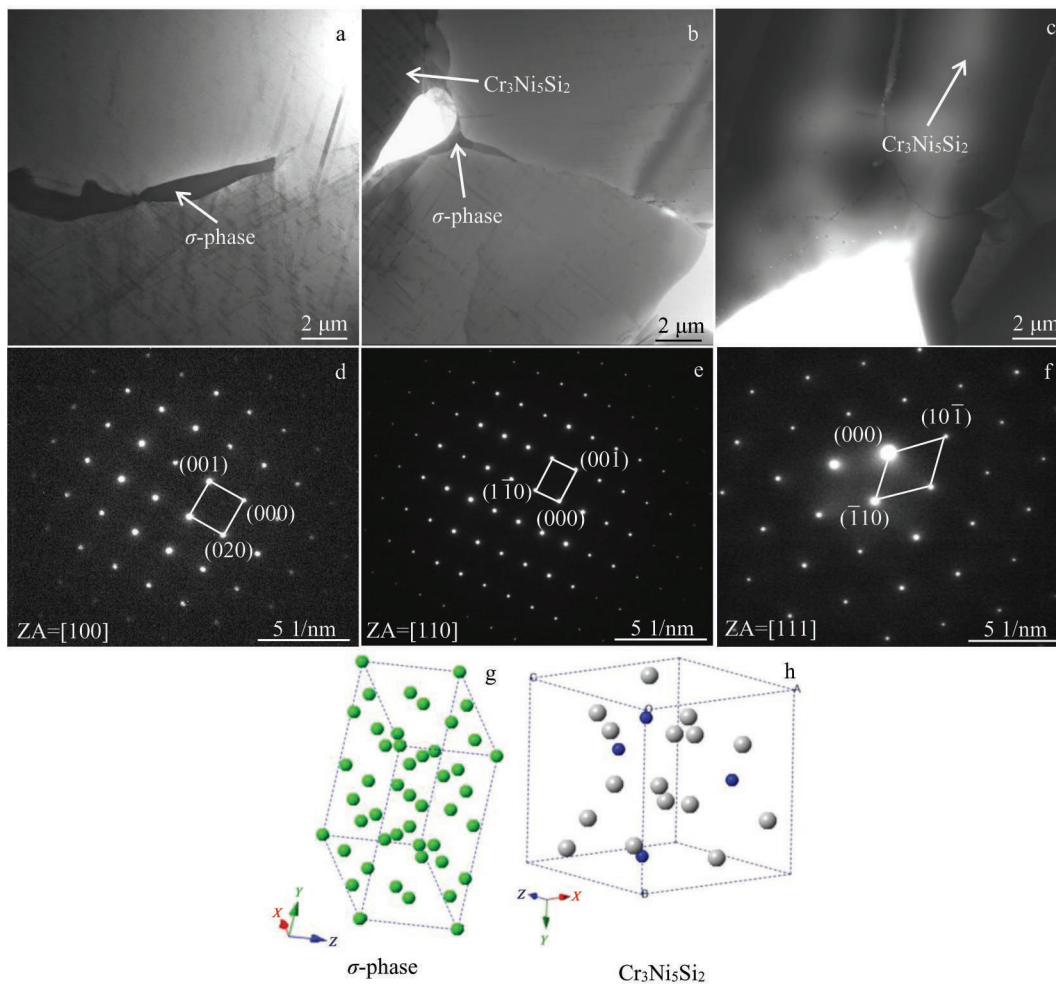


Fig.4 TEM images (a~c) and SAED patterns (d~f) of the precipitates in austenitic stainless steels with different Si contents: (a, d)  $\sigma$ -phase in ZeCor-6wt%Si, (b, e)  $\sigma$ -phases in ZeCor-8wt%Si, and (c, f)  $\text{Cr}_3\text{Ni}_5\text{Si}_2$  phase in ZeCor-8wt%Si; tetragonal structures of  $\sigma$ -phase (g) and  $\text{Cr}_3\text{Ni}_5\text{Si}_2$  phase (h)

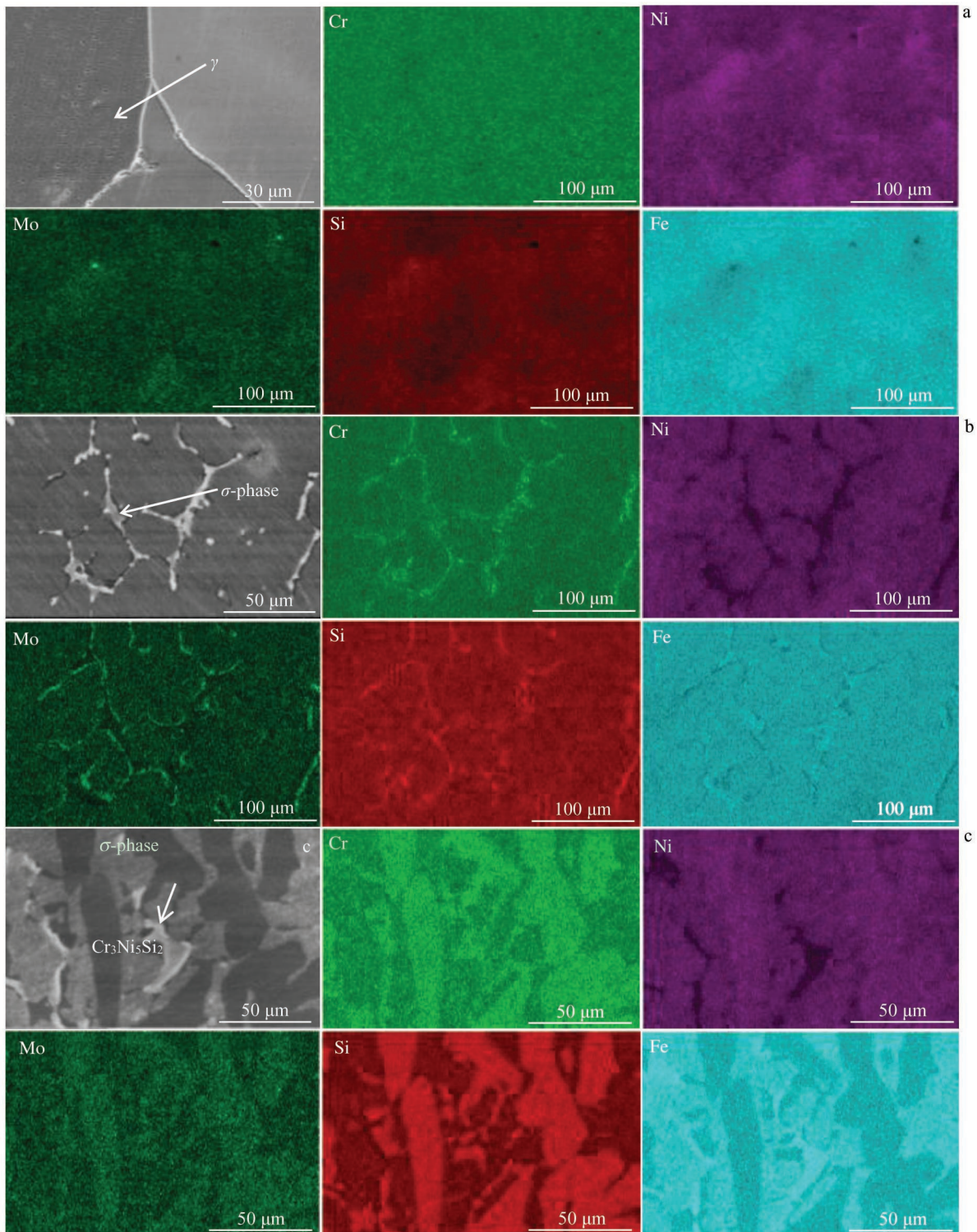


Fig.5 Microstructures and EDS results of ZeCor-4wt%Si (a), ZeCor-6wt%Si (b), and ZeCor-8wt%Si (c)

MPa, which is 1.58 times larger than that of  $\gamma$  matrix and the cracks form in the  $\text{Cr}_3\text{Ni}_5\text{Si}_2$  phase after indentation deformation (Fig. 7d). It can be inferred that the  $\text{Cr}_3\text{Ni}_5\text{Si}_2$  phase is hard and brittle phase, which can hinder the dislocation to enhance the micro-hardness of the  $\gamma$  matrix.

What's more, a schematic diagram of the effect of Si contents and precipitation phases in  $\gamma$  matrix is shown in Fig. 8.

Compared with ZeCor-4wt%Si alloy, the Si atoms solubilized in  $\gamma$  matrix of ZeCor-6wt%Si alloy is increased significantly (Fig. 8a and 8b), which increases the distortion of  $\gamma$  matrix lattice, so that its micro-hardness is improved (Fig. 6). Fig. 8d~8f show the strain area  $A$  of  $\gamma$  matrix in three studied steels. In the hardness test, the applied force ( $F$ ) in  $\gamma$  matrix is a constant value under a loading of 100 g. According to the theory of

elasticity, the  $\sigma$  can be calculated:

$$\varphi = F/A \tag{1}$$

**Table 3** Element contents of matrix and precipitated phases in austenitic stainless steels with different Si contents (wt%)

Element	ZeCor-4wt%Si		ZeCor-6wt%Si		ZeCor-8wt%Si	
	$\gamma$	$\gamma$	$\sigma$ -phase	$\gamma$	$\sigma$ -phase	$Cr_3Ni_5Si_2$
Si	3.49	5.11	8.51	5.43	8.29	10.03
Cr	14.06	13.72	19.03	12.27	15.28	17.17
Ni	15.10	17.42	12.66	16.33	14.15	17.04
Mo	0.82	1.62	5.51	1.13	1.89	2.27
Fe	Bal.	Bal.	Bal.	Bal.	Bal.	Bal.

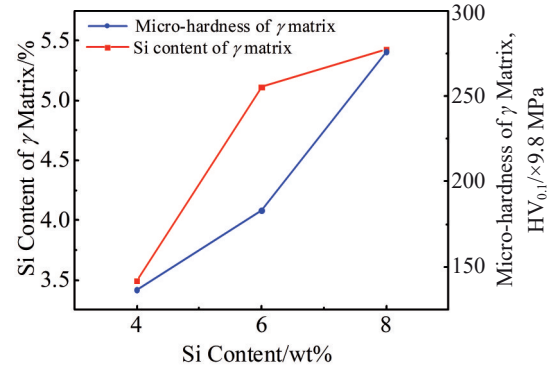


Fig.6 Vickers hardness and Si content of  $\gamma$  matrix for austenitic stainless steel containing 4wt%, 6wt% and 8wt% Si

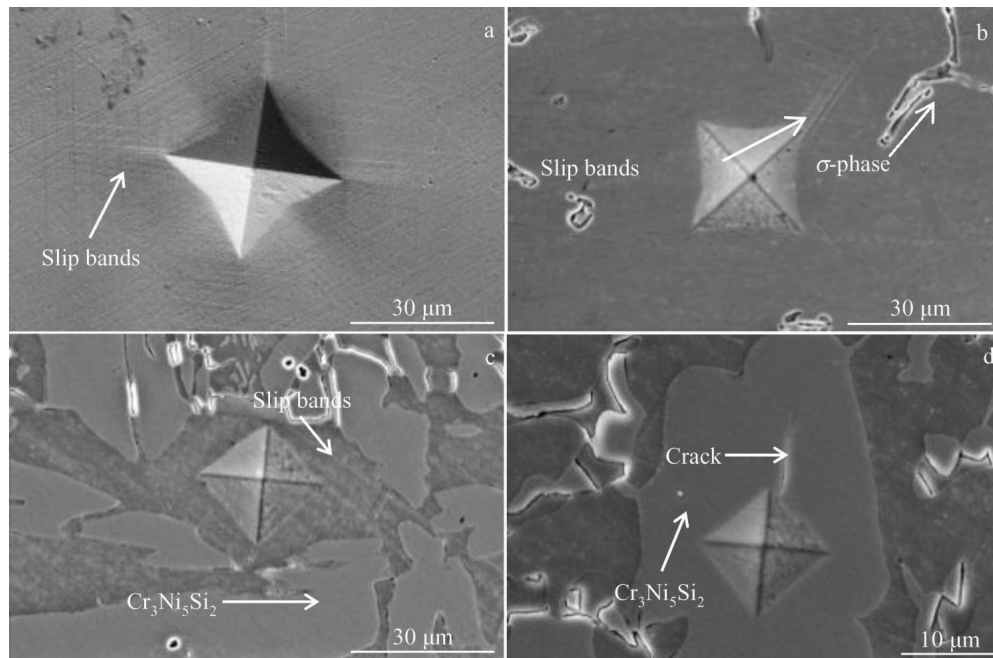


Fig.7 Slip bands around the compression zone on the matrix and precipitates of ZeCor with different silicon contents: micro-hardness indentation on  $\gamma$  matrix of ZeCor-4wt%Si (a), ZeCor-6wt%Si (b), ZeCor-8wt%Si (c), and micro-hardness indentation on  $Cr_3Ni_5Si_2$  (d)

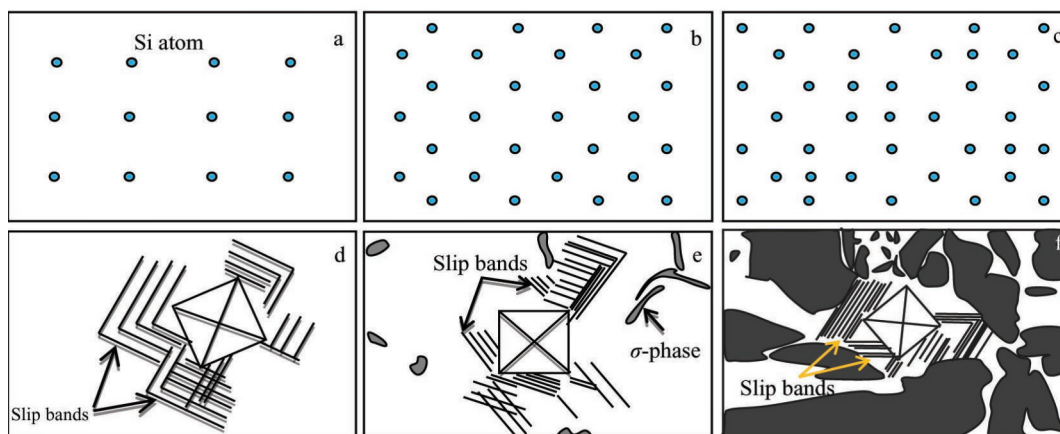


Fig.8 Characteristics of solid solution Si atom and slip lines in matrix of ZeCor-4wt%Si (a, d), ZeCor-6wt%Si (b, e), and ZeCor-8wt%Si (c, f)

where  $\varphi$  is inversely proportional to the force area ( $A$ ). The area  $A$  in ZeCor-6wt%Si is bigger than that in ZeCor-8wt%Si, meaning that  $\varphi_{6\%Si}$  is lower than  $\varphi_{8\%Si}$ . These  $Cr_3Ni_5Si_2$  phases are the main factors resulting in different micro-hardness of  $\gamma$  matrix in ZeCor-6wt%Si alloy and ZeCor-8wt%Si alloy.

### 3 Conclusions

1) The microstructures of ZeCor alloy change with increasing Si contents:  $\gamma$  matrix (4wt% Si)  $\rightarrow$   $\sigma$ -phase and  $\gamma$  matrix (6wt% Si)  $\rightarrow$   $Cr_3Ni_5Si_2$  phase,  $\sigma$ -phase and  $\gamma$  matrix (8wt% Si). The increase in Si content can promote  $Cr_3Ni_5Si_2$  phase formation, but the amount of  $\sigma$ -phase changes little.

2) The  $\sigma$ -phase is mainly precipitated along the grain boundary and enriched with Si, Cr and Mo contents,  $Cr_3Ni_5Si_2$  phase is enriched with Si, Cr, Ni and Mo contents, and in ZeCor-8wt% Si alloy, a large number of  $Cr_3Ni_5Si_2$  phase is precipitated in the  $\gamma$  matrix, which results in lower Cr, Mo content in  $\sigma$ -phase.

3) With the addition of silicon, the solid solution of Si atoms in the  $\gamma$  matrix gradually increases, which increases the degree of distortion of  $\gamma$  matrix lattice, and the  $Cr_3Ni_5Si_2$  phase acts as a hard brittle phase to hinder the dislocation slip. The Si content and the  $Cr_3Ni_5Si_2$  phases are the main factors resulting in the highest micro-hardness of  $\gamma$  matrix in ZeCor-8wt%Si alloy.

### References

- Jin Tao, Nuonok. *Thesis for Master Degree*[D]. Xi'an: Xi'an University of Architecture and Technology, 2007 (in Chinese)
- King Matthew J, William G. *Sulfuric Acid Manufacture*[M]. Netherlands: Elsevier, 2013
- Zhou Yuqin, Gao Zhizheng, Wang Manqing et al. *Sulfuric Acid Production Technology*[M]. Beijing: Metallurgical Industry Press, 2013 (in Chinese)
- Zhang Jiongjiong, Yao Kenan, Chen Han et al. *Rare Metal Materials and Engineering*[J], 2018, 47(6): 1689: 1694
- Stott F H, Wei F I. *Oxidation of Metals*[J], 1989, 369: 391
- Basu S N, Yurek G Y. *Oxidation of Metals*[J], 1991, 281: 315
- Tadaaki Amano. *Corrosion Science*[J], 1993, 885: 891
- Mark A Harper, Robert A Rapp. *Oxidation of Metals*[J], 1994, 303: 333
- Hung Wen Hsu, Tsai Wen Ta. *Materials Chemistry and Physics* [J], 2000, 147: 155
- Ma Yanhong, Huang Yuanwei. *Shanghai Metals*[J], 1999, 21(5): 27: 33 (in Chinese)
- Li Hui, Feng Yunli, Qi Xunjin et al. *Acta Metallurgica Sinica*[J], 2013, 49: 562
- Bratukhin A G, Petrakov A F, Krivonogov G S et al. *Met Sci Heat Treat*[J], 1993, 35: 12
- Burstein G T, Daymond B T. *Corros Sci*[J], 2009, 51: 2249
- Chang Fenghua, Pan Fu. *Boiler Manuf*[J], 1995(1): 64 (in Chinese)
- Du Cuncheng. *Process Equipment & Piping*[J], 2003, 40(2): 54 (in Chinese)
- Liu Huanan. *Sul Acid Ind*[J], 1999(1): 1
- Gang Yimin. *Chem Eng Des*[J], 2004, 14(3): 6
- Li Zhiqiang. *Chem Eng Mach*[J], 1998, 25(1): 50
- Armijo J S, Wilde B C. *Corros Sci*[J], 1968, 8: 649
- Qiu Deliang, Liu Huanan, Zhao Chengyong. *Sulphur Phosphorus & Bulk Materials Handling*[J], 2005(1): 18
- Yu Fuzhou. *Corrosion Resistance of Metal Materials*[M]. Beijing: Science Press, 1982 (in Chinese)
- Yan Xiang. *Thesis for Master Degree*[D]. Wuhan: Huazhong University of Science and Technology, 2004 (in Chinese)
- Ma Yanhong, Huang Yuanwei. *Shanghai Metals*[J], 1999, 9(5): 27 (in Chinese)
- Chen Xiang, Li Yanxiang. *Mater Mech Eng*[J], 2000, 24(2): 14
- Wang Guilin. *Hot Working Technol*[J], 2011, 40(9): 39
- Ou J Y, Wang N X. *Spec Steel*[J], 1981(4): 61
- Liu Huanan, Ye Jixuan. *Sulphur Phosphorus & Bulk Materials Handling*[J], 2007(4): 25
- Lu Chengxu, Yi Haoyu, Liang Tian et al. *Rare Metal Materials and Engineering*[J], 2021, 50(1): 187
- Erich Folkhau. *Stainless Steel Welding Metallurgy*[M]. Beijing: Chemical Industry Press, 2004: 15
- Chen Sihan, Liang Tian, Zhang Long et al. *Acta Metallurgica* [J], 2017, 53(4): 697
- Liu Baosheng, Li Guodong, Wei Yinghui. *Journal of Iron and Steel Research*[J], 2014, 26(1): 1
- Ogundare O, Babatope B, Adetunji A R et al. *J Miner Mater Charact Eng*[J], 2012, 11: 914
- Tomashov N D, Chernova G P. *Passivity and Protection of Metals Against Corrosion*[M]. US: Springer, 1967: 91
- Wang Zhinan, Liang Tian, Zhang Long et al. *Rare Metal Materials and Engineering*[J], 2015, 44(5): 1169
- Wang Yanshu. *Hot Working Technology*[J], 2021, 50(22): 25 (in Chinese)
- Ma Hailin, Li Yan, Geng Zhongrong. *Rare Metal Materials and Engineering*[J], 2015, 44(10): 2373
- Hermas A A, Ogura K, Adachi T. *Electrochimica Acta*[J], 1995, 40(40): 837
- Costa Oliveira F A, Edwards R A H, Fordham R J et al. *Materials & Corrosion*[J], 1990, 41(12): 736
- Qin Zirui, Li Longsheng, Liu Dejing et al. *Sulfuric Acid Engineering Industry*[J], 1996(5): 26
- Qin Zirui, Meng Jiangying, Li Longsheng. *Steel Iron*[J], 1997, 32(12): 46
- Ma Yanhong, Huang Yuanwei. *Material Protection*[J], 2000, 33(5): 7

## 硅对高硅奥氏体不锈钢析出相的影响

李潇欢<sup>1</sup>, 崔国伟<sup>1</sup>, 陈思含<sup>2</sup>, 梁田<sup>2,3,4</sup>, 邢炜伟<sup>2</sup>, 马颖澈<sup>2</sup>, 王平<sup>1</sup>, 吴进明<sup>3</sup>, 李国斌<sup>4</sup>

(1. 东北大学 材料电磁过程研究教育部重点实验室, 辽宁 沈阳 110819)

(2. 中国科学院金属研究所 核材料与安全评价重点实验室, 辽宁 沈阳 110016)

(3. 浙江大学 材料科学与工程学院 硅材料国家重点实验室, 浙江 杭州 310027)

(4. 浙江信得达特种管业有限公司, 浙江 温州 325024)

**摘要:** 采用XRD、TEM和压痕变形等方法研究了Si含量(4%~8%, 质量分数)对高硅奥氏体不锈钢(ZeCor)显微组织的影响。结果表明, Si含量的增加会导致ZeCor合金的相组成发生变化: ZeCor-4%Si合金组织为单相奥氏体( $\gamma$ 相), ZeCor-6%Si合金主要含 $\gamma$ 相和少量 $\sigma$ 相, 在ZeCor-8%Si合金中主要析出 $\text{Cr}_3\text{Ni}_5\text{Si}_2$ 相和少量 $\sigma$ 相。此外,  $\text{Cr}_3\text{Ni}_5\text{Si}_2$ 与 $\sigma$ 相相比具有更高的硅、镍含量。显微硬度HV高达7840 MPa的 $\text{Cr}_3\text{Ni}_5\text{Si}_2$ 相是典型的硬脆相, 该相的析出将大大提高ZeCor-8%Si合金中 $\gamma$ 基体的显微硬度。ZeCor合金中 $\gamma$ 基体的强化机制如下: 固溶强化是ZeCor-6%Si合金的主要强化机制, 而Si的固溶强化和 $\text{Cr}_3\text{Ni}_5\text{Si}_2$ 的析出强化机制都大大提高ZeCor-8%Si合金中的 $\gamma$ 基体的显微硬度。在ZeCor-8%Si合金中,  $\text{Cr}_3\text{Ni}_5\text{Si}_2$ 相起显著作用。

**关键词:** 高硅奥氏体不锈钢; 硅含量;  $\sigma$ 相; 显微硬度测试;  $\text{Cr}_3\text{Ni}_5\text{Si}_2$ 相

**作者简介:** 李潇欢, 女, 1997年生, 硕士生, 东北大学材料电磁过程研究教育部重点实验室, 辽宁 沈阳 110819, 电话: 024-23971986, E-mail: 1900537@stu.neu.edu.cn